Lung nodule type classification in CT images using UNet based segmentation and ANFIS based classification

R.Manickavasagam*, S.Selvan, Mary Selvan*****

**Assistant Professor, Department of BME, Alpha College of Engineering, Chennai INDIA (Tel: +91 90031 65138; e-mail: manick6apr1979@gmail.com).*
***Professor, Department of CSE, St.Peter's Institute of Higher Education and Research, Avadi, Chennai, INDIA* (e-mail:*drselvan@ieee.org*)
**** Assistant Professor, Department of CSE, RMK College of Engineering and Technology, Thiruvallur, INDIA (e-mail: ms.maryselvan@gmail.com*)}

Abstract: The Early detection and classification of lung nodules using computer-aided diagnosis (CAD) is very much needed to reduce mortality rates in lung cancer patients. The spontaneous and accurate classification of lung nodule type is very supportive for the precise lung cancer diagnosis. In this paper, a novel approach is proposed which employs deep learning for segmentation and ANFIS (Adaptive Neuro Fuzzy Inference System) for lung nodule type classification using CT (Computed Tomography) images. The proposed approach uses UNet architecture for the effective ROI segmentation on the LIDC (Lung Image Database Consortium) database images. A modified ANFIS structure using adjustable parameters to choose the contribution of premise parameters to improve classification accuracy is proposed. The Texture, statistical and shape features of the segmented region is extracted using GLCM (Gray-level Co-occurrence Matrix) algorithm. Then ANFIS classifier is employed to classify the nodules into various types such as juxta-pleural, juxta-vascular, well-circumscribed, pleural-tail and ground-glass opacity. The proposed approach is executed in Python platform and performance of the system is evaluated. The results show that the proposed approach achieves sensitivity, accuracy, precision, specificity and AUC (Area under ROC Curve) of 97.18%, 98.87 %, 98.72%, 98.3% and 0.978 respectively under epoch 30. These results are compared with other lung nodule type classification approaches and found to perform better than other approaches.

Keywords: Lung Nodule classification, Computed Tomography (CT), UNet, Adaptive Neuro Fuzzy Inference System (ANFIS), LIDC.

1. INTRODUCTION:

Lung cancer is currently one of the most common causes of death worldwide, with low rates of survival in developing as well as developed countries. According to recent statistics, the survival rate of 5-year is only 16%.It has been estimated that 12 million deaths occur annually related to cancer, of which lung cancer has the major share (Liu et al.,2017). However, the survival rates of lung cancer patients can be improved, if nodules are detected early enough.

Lung nodules are unusual growths in tissues that could denote lung cancer. They are normally round in shape with diameters up to 30 mm. The lung nodules are classified as solid and sub-solid nodules, irrespective of nodule positions. Solid nodules are the most common type of nodules, and they limit the functional characteristics of lung tissues. Sub-solid nodules possess higher thickness than the surrounding tissues and are not visible as they are hidden through bronchovascular structures (Jingjing et al., 2018). Hence, solid nodules are considered for type classification in this work. Solid type lung nodules are characterized as juxta-pleural, juxta-vascular, well-circumscribed, pleural-tail and ground-glass nodules (Ashis et al., 2012). Well-circumscribed nodules are independent and have no extensions into surrounding anatomical structures. Juxta-vascular nodules are observed adjacent to blood vessels. Juxta-pleural nodules are close to adjacent pleural surfaces (Girshick et al., 2014). Pleural-tail nodules have tails that are adherent to the nodules but not to the pleural walls. Ground-Glass Opacity (GGO) nodules are the nodules that have hazy lung areas of slightly increased attenuation without obscuring the bronchial and vascular regions. The accurate classification of lung nodule types will facilitate the precise diagnosis of lung cancer.

To achieve effective lung nodule type classification, various approaches have been proposed (Cao et al., 2016;Kuruvilla et al., 2014;Song et al., 2017;May et al., 2020). These approaches have attained classification of lung nodule type using various segmentation and classification approaches. From the study, it is observed in many cases, that the boundary of the nodules is not clearly defined in the segmented images. If better segmentation is achieved, the accuracy of the classification of nodule type can be improved. For instance, the pleura boundary points of juxta-pleural, pleural-tail nodules will appear in the list of pleura boundary points of nodules because of the connectivity of nodules with the pleura. Hence, the points situated on the pleura boundary need to be removed from the list of pleura boundary points of nodules obtained by tracking endpoints of the lung nodules. The proper boundary identification is essential for accurate classification of the lung nodule types.

Various image segmentation approaches have been employed for classification of lung nodule type such as Adaptive Border Matching (ABM) approach(Shimizu, et al., 2010), Rule Based Region Growing (RBRG) approach(Sousa et al., 2010), Active Contour Method (ACM) (Lee et al., 2010), Adaptive Morphology-based Segmentation Technique (AMST) (Halder et al., 2020) and so on. Recently, deep learning approaches have been proposed for medical image segmentation. The UNet (Ronneberger et al., 2015; Niranjan et al., 2021) is used to capture the background region and obtain accurate localization to identify the ROI. This approach, implemented along with different convolutional layers, provides effective ROI segmentation of input images. This deep learning algorithm outperforms other machine learning based segmentation approaches as they possess specialized architectures and are capable of handling large size of input data and non-linear features.

Various image classification approaches have been used for the classification of lung nodule type such as Ensemble classifier (EC) (Shimizu, et al., 2010), Linear Discriminant Analysis (LDA) (Sousa et al., 2010), Fuzzy C- Means Classifier (FCM) (Lee et al., 2010), Random Forest (RF) classifier (May et al., 2020), Parametric Mixture approach (PMM) (Bin et al., 2013), Support Vector Machine (Halder et al., 2020), TransUnet (Wang et al., 2022), Water Strider optimization Algorithm (WSA) (Saihood et al., 2022) and so on. ANFIS based classifiers (Krim et al., 2018, Zhixian et al., 2014; Manickavasagam et al., 2019; Ricky et al., 2020; Manickavasagam et al., 2022) are employed to obtain better performance in various applications such as renewable energy system, biomedical signal processing, biomedical image classification and so on. This better performance is achieved by the ANFIS classifier by using rule based functions for prediction. ANFIS combines the merits of NN (Neural Network) and FIS (Fuzzy Inference System) to achieve better performance with hybrid learning mechanism.

Improvements in performance measures such as sensitivity, accuracy, precision and specificity are always sought by researchers to make accurate predictions of lung cancer for better treatment options. In this work, a new integrated approach combining UNet for segmentation of lung region and ANFIS for classification of lung nodule type is proposed and this approach is found to yield better performance than other approaches itemised in the literature.

The Introduction section 1 briefs on the related works and the need for this proposed approach for the classification of lung nodule type. In Section 2, the proposed approach is described in detail and Section 3 discusses experimental setup and implementation. In Section 4, the results obtained through simulation are discussed. Section 5 provides the conclusion of this work.

2. DESCRIPTION OF PROPOSED METHOD

The proposed approach is designed in such a way that the combination of deep learning and ANFIS achieves improved accuracy in the classification of lung nodule type. The block diagram of the proposed approach is shown in Figure 1. The lung CT gray scale images from the LIDC/IRDI database (Armato et al., 2011) are preprocessed to obtain images of 512 x 512 size for segmentation.

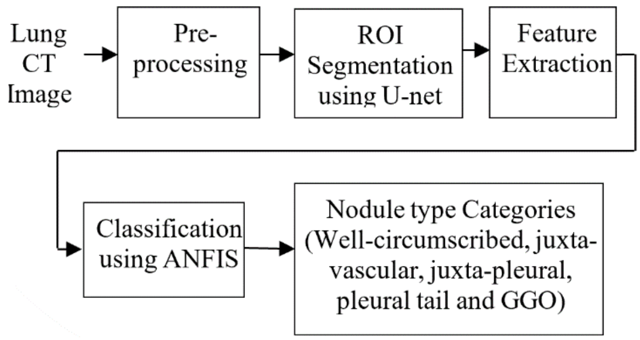

Fig. 1. Block diagram of the proposed integrated approach consisting of UNet and ANFIS.

2.1 ROI Segmentation using UNet

The UNet is a systematic U-shaped network based on convolutional neural network developed for the segmentation of biomedical images to identify the location and content of the selected region. The segmentation obtained using the UNet approach is found to be more accurate, leading to better classification. Hence, this is chosen for the segmentation of CT lung images.

The primary path of UNet consists of max pooling layers along with convolution layers to extract the perception of the input image. The convolution operation is carried out on the input image to split it into small sizes. In convolution layers, the Rectified Linear Unit (ReLu) function (Shin et al., 2016; Krizhevsky et al., 2012) is used to achieve better segmentation. The max pooling operation reduces the size of the convolution layer output.

In secondary path, transposed convolution operation is employed for up-sampling to obtain the output feature map. Then this output is concatenated with the feature map of the same level in the primary path. The UNet architecture used for the segmentation is shown in Figure 2.

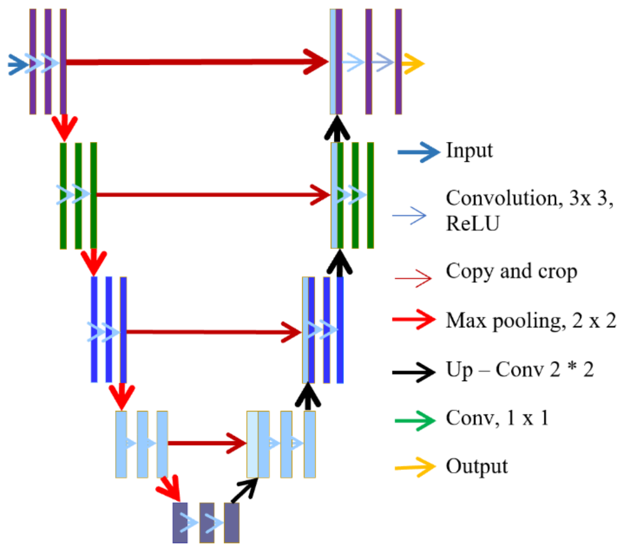

Fig. 2. Proposed UNet structure for segmentation.

In the proposed structure, the primary path comprises of 4 sections and each section consists of two convolution layers and one max pooling layer. The input image with a size of 512 x 512is reduced to 22 x 22 at the end of primary path. The secondary path also contains 4 sections and each section involves one up-sampling layer and two convolution layers. The segmented output image size is increased at the end of secondary path to 292 x 292.The layer specifications of the proposed UNet architecture are given in Table 1.

Table1. Layer Specifications of Proposed UNet architecture

Path	Layer	Input	Kernel	Output
Contracting Path	Convolution	512x512x1	3x3	510x510x16
	Convolution	510x510x16	3x3	508x508x16
	Max pooling	508x508x16	2x2	254x254x16
	Convolution	254x254x16	3x3	252x252x32
	Convolution	252x252x32	3x3	250x250x32
	Max pooling	250x250x32	2x2	125x125x32
	Convolution	125x125x32	3x3	123x123x64
	Convolution	123x123x64	3x3	121x121x64
	Max pooling	121x121x64	2x2	60x60x64
	Convolution	60x60x64	3x3	58x58x128
	Convolution	58x58x128	3x3	56x56x128
	Max pooling	56x56x128	2x2	28x28x128
Bottle neck	Convolution	28x28x128	3x3	26x26x256
	Convolution	26x26x256	3x3	24x24x256
	Convolution	24x24x256	3x3	22x22x256
Expansive Path	Upsampling	22x22x256	2x2	44x44x128
	Convolution	44x44x128	3x3	42x42x128
	Convolution	42x42x128	3x3	40x40x128
	Upsampling	40x40x128	2x2	80x80x64
	Convolution	80x80x64	3x3	78x78x64
	Convolution	78x78x64	3x3	76x76x64
	Upsampling	76x76x64	2x2	152x152x32
	Convolution	152x152x32	3x3	150x150x32
	Convolution	150x150x32	3x3	148x148x32
	Upsampling	148x148x32	2x2	296x296x16
	Convolution	296x296x16	3x3	294x294x16
	Convolution	294x294x16	3x3	292x292x16
Output	Convolution	292x292x16	1x1	292x292x16

The training of UNet structure is explained below. The dataset images with corresponding pixel-level annotations (Ground truth) are used for training. The weights and biases that are associated with the convolutional layers are initialized. These parameters are modified during the training process to optimize the performance of the network for segmentation. The training set images are given to the UNet with a batch size of 80. For each batch, the predicted segmentation map is obtained using a forward pass. Then the loss between the ground truth and predicted segmentation map is obtained using the cross entropy loss function (Michael et al., 2022). The parameters of the convolution layer filters are updated using the stochastic gradient descent (SGD) algorithm through back propagation. This process is repeated for a number of iterations to minimize the loss to less than 0.01.

2.2 Feature Extraction

Feature extraction is the process of representing the characteristics of ROI regions to form the feature set, which is extracted from the segmented lung region of CT images. The features of the segmented lung region such as texture, statistical and shape features provide domain specific features in the spatial regions of the detected lung area. Since shape and texture features have potential orientation in terms of coordinates and are suitable for various lung CT image datasets, they are considered for classification. The statistical features of an image provide the maximum information about the spatial relationships. The Gray-level Co-occurrence Matrix (GLCM) (Haralick et al., 1973) approach is found to be an efficient approach, offering better spatial relation of the pixels for different orientations in order to represent the visual perceptions of the segmented lung region. Hence, the GLCM approach to feature extraction is used in this work. The details of texture, statistical and shape features are given in Table 2.

Table 2. Details of Texture, Statistical and Shape Features used for classification

Sl. No	Feature Type	Features	
1	Texture Features	1. Homogeneity 2. Autocorrelation 3. Energy 4. Entropy 5. Contrast 6. Maximal correlation coefficient 7. Correlation 8. Shade 9. Prominence 10.Maximum Probability 11.Autocorrelation1	12. Angular second moment 13. Inverse Difference moment 14. Inertia 15. Sum Variance 16. Difference Variance 17. Inverse Difference 18. Dissimilarity 19. Sum Average 20. Information Measure of Correlation 21. Sum Entropy 22. Difference Entropy
2	Shape Features	1. Perimeter 2. Area 3. Eccentricity 4. Major Axis Length	5. Extent 6. Minor Axis Length 7. Equivalent Diameter
3	Statistical Features	1. Mean 2. Variance 3. Standard deviation	

2.3 Classification using ANFIS

The ANFIS classifier has fast convergence rate with automatic parameter tuning and produces smoothness in output compared to the conventional neural network classifier (Ricky et al., 2020). The proposed ANFIS structure (Jang et al., 1993) is constructed with 5 layers such as fuzzification, product, normalization, defuzzification and output layers. 32 features extracted from segmented ROI, provided in Table 2, are given as input to the ANFIS classifier. The proposed ANFIS structure is modified to include adjustable parameters 'j_k' in layer 2 to improve classification accuracy. This is done to choose the contribution of the premise parameters of various inputs to reduce the classification error, which increases the classification accuracy. The representation of the sample ANFIS structure for 2 inputs used for the classification of lung nodule type is shown in Figure 3. For better understanding, only 2 inputs are considered for explaining the operations involved. However, the actual ANFIS structure used in this work has 32 inputs.

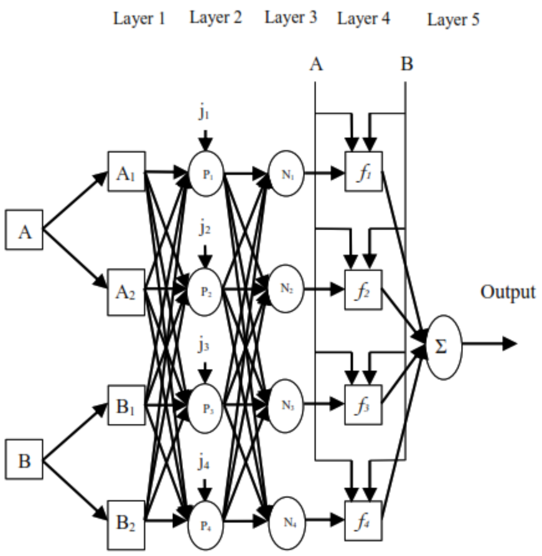

Fig. 3. Representation of ANFIS structure for 2 inputs used for Lung Nodule type Classification.

Layer 1: Everynode i in this layer has output O_i^1 represented in Equation (1) and Equation (2):

$$O_i^1 = \mu_{A_i}(A) \qquad i=1,2 \qquad (1)$$

$$O_i^1 = \mu_{B_i}(B) \qquad i=3,4 \qquad (2)$$

where A, B are the input of node i; A_i, B_i are the linguistic label (Low, High) associated with the node function and μ_{A_i}, μ_{B_i} are the bell shaped membership functions:

$$\mu_{A_i}(A) = \frac{1}{1+\left(\frac{A-c_i}{a_i}\right)^{2b_i}} \qquad (3)$$

$$\mu_{B_i}(A) = \frac{1}{1+\left(\frac{B-c_i}{a_i}\right)^{2b_i}} \qquad (4)$$

Where$\{a_i,\ b_i,\ c_i\}$ is the premise parameter set used to vary the bell shaped function, where i=1,2for input A and i=3,4 for input B.

Layer 2: Everynode in layer 2 multiplies (AND operation) the inputs with adjustable parameter 'j_k' given as follows:

$$w_1 = \mu_{A_1}(A) * \mu_{B_1}(B) * j_1 \qquad (5)$$

$$w_2 = \mu_{A_1}(A) * \mu_{B_2}(B) * j_2 \qquad (6)$$

$$w_3 = \mu_{A_2}(A) * \mu_{B_1}(B) * j_3 \qquad (7)$$

$$w_4 = \mu_{A_2}(A) * \mu_{B_2}(B) * j_4 \qquad (8)$$

Where, A and B are the inputs and '*' denotes AND operation Where, μ_{A_1},μ_{A_2},μ_{B_1},μ_{B_2} are bell shaped membership functions for A_Low, A_High, B_Low and B_High respectively.

j1, j2, j3, j4 – adjustable parameters used to choose the contribution of premise parameters; $0 < j < 1$, j1 + j2 =1 and j3 + j4 =1

w1, w2, w3, w4– Outputs of layer 2

The values 'j_k' are set to achieve improved classification accuracy of nodule types. For every output class, the values of 'j_k' are modified to reduce the error below 0.001. This procedure of varying the contribution of premise parameters improves the accuracy of classification.

Layer 3: Normalized weights used for faster convergence to speed up learning are determined as shown in Equation (9):

$$\overline{w_i} = \frac{w_i}{\sum_{i=1}^{N} w_i} \quad i = 1,2..N; N = 4 \qquad (9)$$

where N – number of nodes in layer 3.

Layer 4: The output of each node in this layer is determined using Equation (10):

$$O_i^4 = \overline{w_i} f_i = \overline{w_i}\,(p_i A + q_i B + r_i) \qquad (10)$$

wherep_i, q_i, r_i - consequent parameter set

$f_i -$ function for linear combinations of consequent parameters, i=1,2,3,4

Layer 5: The overall output is shown in Equation (11):

$$O_1^5 = \sum_{i=1}^{N} Y_i = \sum_{i=1}^{N} \overline{w_i} f_i \quad (11)$$

Wherev_i- Output of node i of layer 4

The rules formedforthe2 input ANFIS structure are given below,

If A_Low AND B_Low, then f1 = p1A + q1B + r1

If A_Low AND B_High, then f2 = p2A + q2B + r2

If A_High AND B_Low, then f3 = p3A + q3B + r3

If A_High AND B_High, then f4 = p4A + q4B + r4

The actual output is calculated using the relation (11). The target output is obtained from the annotations of the database. The input is applied to layer 1. Hybrid learning Algorithm is used for determining the premise parameters and consequent parameters. The hybrid training algorithm has two passes such as forward pass and backward pass. In forward pass, initial consequent parameters and premise parameters are assumed. The input Features pass through various layers to yield an output. This output is compared with the target output to obtain the error in layer 5. Then, in the backward pass, the error is propagantes backwards from the output to the input. In layer 4 using the least square approach, the consequent parameters are changed to decrease the error. In layer 1, using the gradient decent approach, the premise parameters are updated to decrease the error. This procedure is repeated till the error is reduced below 0.001.

The error is calculated using Equation (12):

$$E = (T - Y)^2 \tag{12}$$

Where, T – Target Output and Y – Actual Output

The minimization of error in nodes of layer 4 is attained using least square approach with following conditions.

$$\frac{\partial E}{\partial p_i} = 0; \qquad \frac{\partial E}{\partial q_i} = 0; \qquad \frac{\partial E}{\partial r_i} = 0; \qquad i=1,2,3,4$$

where, p_i, q_i, r_i are consequent parameters.

The consequent parameters p_i, q_i, r_i are calculated using Equation (13): [See Appendix for the derivation]

$$\begin{pmatrix} p_1 \\ p_2 \\ p_3 \\ p_4 \\ q_1 \\ q_2 \\ q_3 \\ q_4 \\ r_1 \\ r_2 \\ r_3 \\ r_4 \end{pmatrix} = \begin{pmatrix} A_1 & A_1 & A_2 & A_2 & B_1 & B_2 & B_1 & B_2 & 1 & 1 & 1 & 1 \\ A_1 & A_1 & A_2 & A_2 & B_1 & B_2 & B_1 & B_2 & 1 & 1 & 1 & 1 \\ A_1 & A_1 & A_2 & A_2 & B_1 & B_2 & B_1 & B_2 & 1 & 1 & 1 & 1 \\ A_1 & A_1 & A_2 & A_2 & B_1 & B_2 & B_1 & B_2 & 1 & 1 & 1 & 1 \\ A_1 & A_1 & A_2 & A_2 & B_1 & B_2 & B_1 & B_2 & 1 & 1 & 1 & 1 \\ A_1 & A_1 & A_2 & A_2 & B_1 & B_2 & B_1 & B_2 & 1 & 1 & 1 & 1 \\ A_1 & A_1 & A_2 & A_2 & B_1 & B_2 & B_1 & B_2 & 1 & 1 & 1 & 1 \\ A_1 & A_1 & A_2 & A_2 & B_1 & B_2 & B_1 & B_2 & 1 & 1 & 1 & 1 \\ A_1 & A_1 & A_2 & A_2 & B_1 & B_2 & B_1 & B_2 & 1 & 1 & 1 & 1 \\ A_1 & A_1 & A_2 & A_2 & B_1 & B_2 & B_1 & B_2 & 1 & 1 & 1 & 1 \\ A_1 & A_1 & A_2 & A_2 & B_1 & B_2 & B_1 & B_2 & 1 & 1 & 1 & 1 \\ A_1 & A_1 & A_2 & A_2 & B_1 & B_2 & B_1 & B_2 & 1 & 1 & 1 & 1 \end{pmatrix}^{-1} \begin{pmatrix} T \\ T \\ T \\ T \\ T \\ T \\ T \\ T \\ T \\ T \\ T \\ T \end{pmatrix} \tag{13}$$

where, A_1, A_2, B_1, B_2 are inputs; T- Target output

Now the problem is to identify the values of the premise parameters a_i, b_i and c_i of inputs.

The premise parameters a_i, b_i and c_i (which control the Membership function) and the consequent parameters p_i, q_i and r_i (which control the output) are to be chosen to minimize the error. The error is to be minimized to achieve accurate classification. The values of premise parameters are chosen using Gradient Descent algorithm as shown in relation (14):

$$Gradient\ of\ Error = \frac{\partial E}{\partial (A,B)} \tag{14}$$

Where E – Error, A and B are inputs

Using Gradient Descent algorithm, the premise parameter a_i is updated using the relation:

$$a_i\,(n+1) = a_i(n) - \eta \frac{\partial E}{\partial a_i} \tag{15}$$

Where, $a_i\,(n+1)$ - Updatedvalueof premise parameter 'a_i'

$a_i(n)$ - Present value of premise parameter 'a_i'

η – learning rate

A - Input

Premise parameters b_i and c_i of input A are updated (i=1,2) using similar relations as given in (15). Also the premise parameters a_i, b_i and c_i for input B (i=3,4) are updated. The output is calculated with updated premise parameters. These steps are repeated for the number of epochs to decrease the error to be less than 0.001. The learning outcomes of ANFIS training are premise parameters a_i, b_i and c_i of node i (i =1,2, 3,4) in layer 1 and consequent parameters p_i, q_i and r_i of node i (i =1,2,3,4) in layer 4. Based on the experimentation, the learning rate considered for training is 0.8. Here, bell shaped membership function with two level linguistic variables is used for the implementation.

3. IMPLEMENTATION

The proposed approach is executed in Python 3.7.4. The implementation platform uses keras 2.1.3 with tensorflow as backend along with CPU acceleration. The simulations are done with three different ratios of training and testing sample sets such as 50 - 50, 60 - 40 and 70 -30 percentages to evaluate the performance of the proposed system.

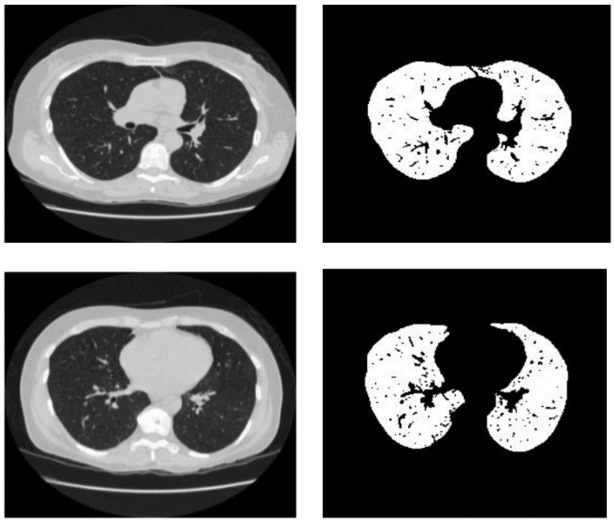

(a) (b)

Fig. 4. (a) Sample Input CT images (b) Sample Segmented Output images from UNet.

3.1 Dataset

The lung CT images from the Lung Image Database Consortium (LIDC) (Armato et al., 2011) are used for validating the proposed approach. This database consists of 1018 images of non-nodules and nodules with mínimum nodule Diameter of 3 mm along with its annotations. Among the 1018 images, 135 images do not have nodules and the remaining 883 images have 2669 nodules. Out of these 883 images, 204 images have well-circumscribed nodules, 396 images have juxta-vascular nodules, 129 images have juxta-pleural nodules, 88 images have pleural-tail nodules and 66 images have ground-glass opacity nodules. The experiments are conducted with various numbers of input images and epochs to analyze the performance of the proposed approach. The sample Segmented images along with input CT images are shown in Figure 4.

3.2 Performance Metrics

The performance evaluation Metrics considered are sensitivity, accuracy, precision and specificity. Receiver Operating Characteristics (ROC), which is used to find the overall performance of the classifier, is plotted between False Positive Rate (FPR) and True Positive Rate (TPR). From this, Area under the ROC Curve (AUC) is calculated, which represents the cumulative Measure of performance for all posible classifications.

4. RESULTS AND DISCUSSION

This work incorporates an integration of UNet for ROI segmentation of the lung region and ANFIS classifier for classifying the lung nodule type based on the Feature values from the Segmented image.

The Accuracy of the proposed approach for various training and testing ratios and epochs is shown in Figure 6. Figure 7 shows the sensitivity of the proposed approach for various training and testing ratios and epochs. Figure 8 and Figure 9 show the specificity and precision respectively of the proposed approach for various training and testing ratios and epochs.

It is observed in Figures 5, 6, 7 and 8 that when the number of epochs is increased beyond 30, the improvements in various performance measures are not very significant. Hence, epoch 30 is chosen for further implementation. Also, it can be seen that reasonably good results are obtained for 50% - 50% of the training and testing set. When the ratio of training and testing set is increased, the performance measures are increased as expected.

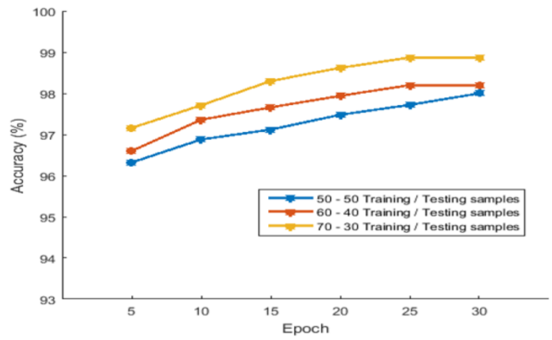

Fig. 5. Accuracy vs Epoch for various training and testing set ratios.

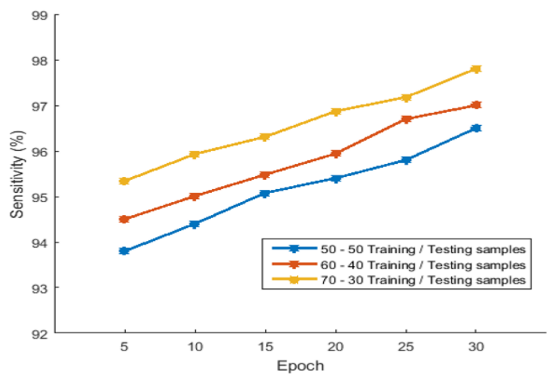

Fig. 6. Sensitivity vs Epoch for various training and testing set ratios.

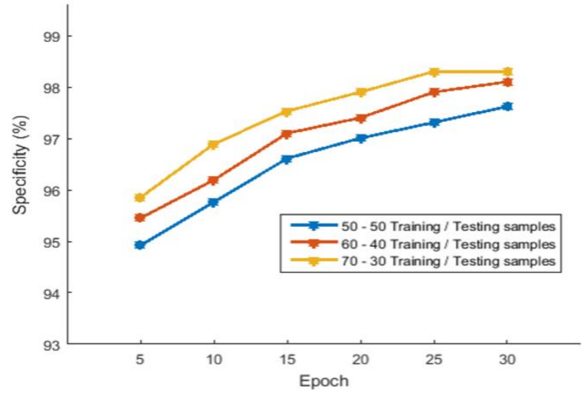

Fig. 7. Specificity vs Epoch for various training and testing set ratios.

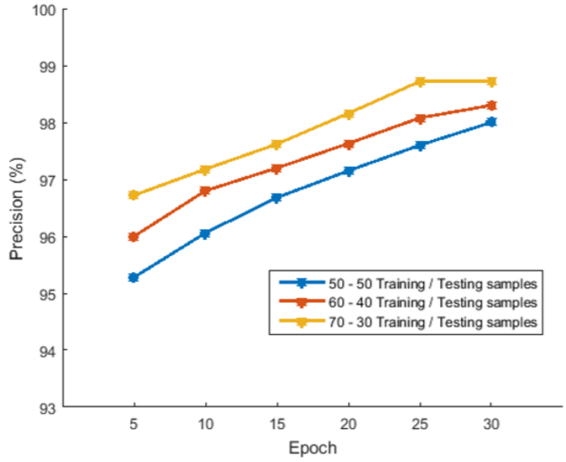

Fig. 8. Precision vs Epoch for various training and testing set ratios.

The ROC curve denotes the performance of classification plotted between False Positive Rate (FPR) and True Positive Rate (TPR), where TPR is same as sensitivity and FPR is 1 – specificity. The comparison of ROC curves of proposed approach for various testing and training set ratios is shown in Figure 9. The AUC value achieved for 70% - 30% training and testing set ratio is 0.978, which indicates the overall performance of the prediction for epoch 30.

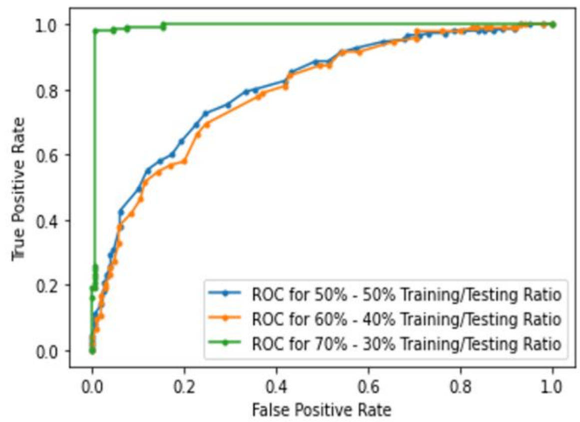

Fig. 9. ROC curves for various training and testing set ratios.

Table 3 shows the computational time of proposed approach for various training and testing set ratios.

The proposed approach achieves the computation time of 56.27 minutes for training and 42.56 seconds for testing for 70% - 30% training testing set ratio for epoch 30.

Table 3. Computation time for various training and testing set ratios

Training and testing set ratio (%)	Overall Computation Time (CT) for training (Minutes)	Average CT for one image for testing (Seconds)
50 - 50	38.23	63.42
60 - 40	43.26	55.28
70 - 30	56.27	42.56

The confusion matrix obtained for the 70 % – 30 % of training and testing sample set is given in Figure 10. It shows that very few images are wrongly classified by the proposed approach.

Output Classes \ Target Classes	Well-circumscribed	Juxta-vascular	Juxta-pleural	Pleural tail	GGO	No Nodules
Well-circumscribed	60	1	0	0	0	0
Juxta-vascular	0	117	1	0	1	0
Juxta-pleural	0	0	38	1	0	0
Pleural tail	0	0	0	26	0	0
GGO	0	0	0	0	20	0
No Nodules	1	0	1	0	0	39

Fig. 10. Confusion matrix for 70 - 30 training and testing set ratio.

(Bin et al., 2013) proposed Fuzzy Integrated Active Contour Model with Support Vector Machine Classifier approach for pulmonary nodule classification. (Liu et al., 2018) proposed multi-scale CNN approach for the type classification of lung nodule. (Halder et al., 2020) proposed adaptive morphology-based segmentation technique and Support Vector Machine for lung nodule segmentation and detection. (Wang et al., 2022) proposed TransUNet based lung nodule classification. (Saihood et al., 2022) proposed fusión based lung nodule classification using Ostu and water Strider approaches. The proposed approach is compared with the approaches proposed by (Bin et al., 2013; Liu et al., 2018; Halder et al., 2020; Wang et al., 2022; Saihood et al., 2022). The results are shown in Table 4. For all the approaches, 70% - 30% training and testing ratio is used.

From the results shown in Table 4, it is seen that the proposed approach outperforms other approaches. The sensitivity, accuracy, precision, specificity and AUC of the proposed approach are 97.18 %, 98.87 %, 98.72%, 98.3% and 0.978 respectively which are better than other approaches. Also, our approach has considered all the images in the database LIDC/IDRI where as other approaches have considered slightly less number of images for their implementation.

Table 4. Comparison of performance measures of the proposed approach with other approaches

Approach	Performance				
	Accuracy (%)	Sensitivity (%)	Specificity (%)	Precision (%)	AUC
FIACM + SVM (Bin et. al.)	94.9	87.5	96.8	94.81	0.916
CNN (Liu et. al.)	90.3	86.6	89.2	-	-
AMST+SVM (Halder et. al.)	94.27	94.88	93.45	-	-
TransUNet (Wang et. al.)	84.6	70.9	93.2	-	0.862
GLCM fusión +Ostu+WSA (Saihood et. al.)	97.3	96	98	-	0.949
UNet + ANFIS [Proposed]	98.87	97.18	98.3	98.72	0.978

5. LIMITATION

In the present work, the training and testing ratio of 70% - 30% was used as in various other works. When we tested our results for the different training and testing ratios, we observed a degradation in accuracy. In the proposed ANFIS structure, adjustable parameters 'j_k' were used to choose the contribution of premise parameters to improve classification accuracy. The values of 'j_k' are chosen based on experimentation with a trial and error approach. To further improve accuracy of classification for all training and testing ratios, the values of 'j_k' are to be chosen properly. In our work, two linguistic variables are used and hence two adjustable parameters for every input are chosen to improve the accuracy. If we choose three linguistic variables, three adjustable parameters can be used and hence there is a possibility for further improving the classification accuracy. Also, instead of trial and error the adjustable parameters can be chosen by employing a suitable optimization technique.

6. CONCLUSION

A novel approach, considering the UNet approach for segmentation and ANFIS for classification is proposed for the classification of lung nodule types from the LIDC-IDRI database. The proposed ANFIS structure is modified to include adjustable parameters 'j_k' in layer 2 to improve classification accuracy. This is done to choose the contribution of the premise parameters of various inputs to reduce the classification error, which increases the classification accuracy. The experimental results show that the proposed approach performs better compared with other approaches. Sensitivity, accuracy, precision, specificity and

AUC of the proposed approach are 97.18 %, 98.87 %, 98.72%, 98.3% and 0.978 respectively under epoch 30 for 70% - 30% training and testing ratios. When tested for other training and testing ratios degradation was observed in the performance. A suitable optimization Technique may be employed to choose the adjustable parameters ‘j_k’ effectively to improve the classification accuracy. Other image formats, such as MRI and PET-CT can be used for lung nodule type classification. Attempt could be made to use this approach for the classification of other cancer nodules.

Conflict of Interest: On behalf of all authors, the corresponding autor states that there is no conflicto of interest.

REFERENCES

Armato S. G, McLennan G, Bidaut L. (2011). The lung image database consortium (LIDC) and image database resource initiative (IDRI): a completed reference database of lung nodules on CT scans. *Medical Physics*, 38(2): pp. 915–931.

Ashis Kumar Dhara, Sudipta Mukhopadhyay, Niranjan Khandelwal. (2012). Computer-aided Detection and Analysis of Pulmonary Nodule from CT Images: A Survey. *IETE Technical Review*, 29(4): pp. 265-275.

Bin Li, Kan Chen, Lianfang Tian, Yao Yeboah, Shanxing Ou. (2013). Detection of Pulmonary Nodules in CT Images Based on Fuzzy Integrated Active Contour Model and Hybrid Parametric Mixture Model. *Computational and Mathematical Methods in Medicine*, 2013: pp. 1-15, 2013.

Cao, Hong Liu, Enmin Song, Guangzhi Ma, Xiangyang Xu, Renchao Jin, Tengying Liu, Chih-Cheng Hung. (2016). Two-Stage Convolutional Neural Network Architecture for Lung Nodule Detection. *Computer methods and programs in biomedicine*, 124: pp. 91-107.

Doi K. (2007). Computer-aided diagnosis in medical imaging: historical review, current status and future potential. *Computerized Medical Imaging and Graphics*, 31(4): pp. 198–211.

Girshick R, Donahue J, Darrell T, Malik J: Rich feature hierarchies for accurate object detection and semantic segmentation. (2014). *Proceedings of the IEEE Conference on Computer Vision and Pattern Recognition*, pp. 580–587.

Halder A., Chatterjee S., Dey D., Kole S, Munshi S. (2020). An adaptive Morphology based segmentation Technique for lung nodule classification in thoracic CT image. *Computer Methods and Programs in Biomedicine*, 197:1.14.

Haralick M, Shanmugam Hak Dinstein K. (1973). Textural Features for Image Classification. *IEEE Transactions on Systems, Man and Cybernetics, SMC* - 3(6): pp. 610-621.

Jang Jyh-Shing Roger. (1993). ANFIS: Adaptive –Network – Based Fuzzy Inference System. *IEEE Transactions on Systems, Man and Cybernetics*, 23(3): pp. 665-685.

Jingjing Yuan, Xinglong Liu, FeiHou, Hong Qin, Aimin Hao. (2018). Hybrid-feature-guided Lung nodule type classification on CT images. *Computers & Graphics*, 70: pp. 288 – 299.

Krim F, Mellit A, Talbi B, Arabi A. (2018). Multiclass adaptive neuro-fuzzy classifier and feature selection techniques for photovoltaic array fault detection and classification. *Renewable Energy*, 127: pp. 548-558.

Krizhevsky A, Sutskever L, Hinton G. E. (2012). Imagenet classification with deep convolutional neural networks. *Advances in Neural Information Processing Systems*, 2012: pp. 1097– 1105.

Kuhnigk J.M, Dicken V, Bornemann L, Bakai A, Wormanns D, Krass S, Peitgen HO. (2006). Morphological segmentation and partial volume analysis for volumetry of solid pulmonary lesions in thoracic CT scans. *IEEE Transactions on Medical Imaging*. 25(4): pp. 417– 434.

Kuruvilla J, Gunavathi K. (2014). Lung cancer classification using neural networks for CT images. *Computer Methods and Programs in Biomedicine*, 113(1): pp. 202–209.

Lee S.L, Kouzani A.Z, Hu E.J. (2010). Random forest based lung nodule classification aided by clustering. *Computerized Medical Imaging and Graphics*, 34: pp. 535-542.

LIDC-IDRI, https://wiki.cancerimagingarchive.net/display/Public/LIDC-IDRI.

Liu J, Jiang H, Gao M. (2017). An assisted diagnosis system for detection of early pulmonary nodule in computed tomography images. *Journal of Medical Systems*, 41(2): pp. 30–43.

Liu X, Hou F, Qin H, Hao A. (2018). Multi-view multi-scale CNNs for lung nodule type classification from CT images. *Pattern Recognition*, 77: pp. 262-275.

Manickavasagam R, Selvan S. (2019) Automatic detection and classification of lung nodule in CT images using optimized neuro fuzzy classifier with cuckoo search Algorithm. *Journal of Medical Systems*, vol. 43, issue 3(77), pp.1-9.

Manickavasagam R, Selvan S, Mary Selvan. (2022) CAD system for lung nodule detection using deep learning with CNN. *Medical & Biological Engineering & Computing*, vol. 60, issue 1, pp.221 - 228.

May Phu P, Sarinporn Visitsattapongse, Kazuhiko Hamamoto, Supan T, Chuchart P. (2020). Automatic Detection of Pulmonary Nodules using Three-dimensional Chain Coding and Optimized Random Forest. *Applied Sciences*, 10 (2348): pp. 1 – 25.

Michael Yeung, Evis Sala, Carola-Bibiane Schonalieb, Leonardo Rundo. (2002). Unified Focal Loss: Generating Dice and Cross entropy-based losses to handle class imbalanced medical image segmentation. Computerized Medical Imaging and Graphics, 95: pp. 1-13.

Monireh Sheikh Hosseini, Maryam Zekri. (2012). Review of Medical Image Classification using the Adaptive Neuro-Fuzzy Inference System. *Journal of Medical Signals and Sensors*, 2: pp. 21-28.

Niranjan Kumar S, Malin Bruntha P, Isaac Daniel S, Ajay Kirubakar J, Elaine Kiruba R, Siril Sam, Immanuel Alex Pandian S. (2021). Lung Nodule Segmentation Using UNet, *International Conference on Advanced*

Computing and Communication Systems, 2021: pp. 420 -424.

Panpan Wu, XuanchaoSun, Ziping Zhao, Haishuai Wang, Shirui Pan, Bjorn Schuller. (2020). Classification of Lung Nodules Based on Deep Residual Networks and Migration Learning. *Computational Intelligence and Neuroscience*, 2020: pp. 1 – 10.

Ricky Mohanty, Sandeep Singh S., Pradeep Kumar Mallick, Subhendu Kumar Pani. (2020). A Classification Model Based on an Adaptive Neuro-fuzzy Inference System for Disease Prediction. *Bio-inspired Neurocomputing*, 2020: pp. 131-149.

Ronneberger O, Fischer P, Brox T: U-net. (2015). Convolutional networks for biomedical image segmentation. *International Conference on Medical image computing and computer-assisted intervention*. Springer, 2015: pp. 234–241.

Saihood A, Karshenas H, Reza Naghsh Nilchi A. (2022). Deep fusión of gray levelco-occurrence matrices for lung nodule classification, *PLoS ONE*, 17 (9): 1-26.

Shimizu, Nakagomi K, Narihira T, Kobatake H, Nawano S, Shinozaki K. (2010). Automated segmentation and classification of 3D CT images based on statistical atlas and graph cuts. *Proceedings of MCV*, 2010:pp. 129-138.

Shin H. C, Roth H. R, Gao M. (2016). Deep convolutional neural networks for computer-aided detection: CNN architectures, dataset characteristics and transfer learning. *IEEE Transactions on Medical Imaging*, 35(5): pp. 1285–1298.

Song Q, Zhao L, Luo X, Dou X. (2017). Using deep learning for classification of lung nodules on computed tomography images. *Journal of Healthcare Engineering*, 2017: pp. 1-7.

Sousa J.R, Silva A.C, Paiva A.C, Nunes R.A. (2010). Methodology for automatic detection of lung nodules in Computerized Tomography images. *Computer Methods and Programs in Biomedicine*, 98: pp. 1-14.

Wang H, Zhu H, Ding L. (2022). Accurate classification of lung nodules on CT images using the TransUnet, *Frontiers in PublicHealth*, 2022: pp.1-9.

Zhixian Yang, Yinghua Wang, Gaoxiang Ouyang. (2014). Adaptive Neuro-Fuzzy Inference System for Classification of Background EEG Signals from ESES Patients and Control. *Machine Learning for Medical Applications*, 2014: pp. 1 – 14.

APPENDIX

The derivation of estimation of consequent parameters p_i, q_i *and* r_i using least square method is shown here.

The output of node 1 of layer 4 with respect to consequent parameters p_1, q_1 *and* r_1 is,

$$Y_1 = (p_1A_1 + q_1B_1 + r_1) \quad \textbf{(A.1)}$$

Where p_1, q_1 *and* r_1 are consequent parameters of node 1.

The Output of layer 5,

$$O_1^5 = \sum_{i=1}^{4} Y_i \quad \textbf{(A.2)}$$

The error in layer 5 is estimated using the relation,

$$E = (T - \sum_{i=1}^{4} Y_i)^2 \quad \textbf{(A.3)}$$

$$E = [T - \sum_{i=1}^{2}(p_iA_i + q_iB_i + r_i) - \sum_{i=3}^{4}(p_iA_i + q_iB_{i-2} + r_i)]^2 \textbf{(A.4)}$$

$$E = [T - \{(p_1A_1 + q_1B_1 + r_1 + p_2A_1 + q_2B_2 + r_2) + (p_3A_2 + q_3B_1 + r_3 + p_4A_2 + q_4B_2 + r_4)\}]^2 \quad \textbf{(A.5)}$$

The goal is to find the values of p_i, q_i, r_i that minimize the error.

To minimize the error with respect to p_1, q_1, r_1, we have the following conditions

$$\frac{\partial E}{\partial p_1} = 0; \qquad \frac{\partial E}{\partial q_1} = 0; \qquad \frac{\partial E}{\partial r_1} = 0;$$

$$\frac{\partial E}{\partial p_1} = 2\{T - [(p_1A_1 + q_1B_1 + r_1 + p_2A_1 + q_2B_2 + r_2) + (p_3A_2 + q_3B_1 + r_3 + p_4A_2 + q_4B_2 + r_4)]\}(-A_1) = 0 \ \textbf{(A.6)}$$

$$2A_1\{-T + [(p_1A_1 + q_1B_1 + r_1 + p_2A_1 + q_2B_2 + r_2) + (p_3A_2 + q_3B_1 + r_3 + p_4A_2 + q_4B_2 + r_4)]\} = 0 \textbf{(A.7)}$$

$$\{-T + [(p_1A_1 + q_1B_1 + r_1 + p_2A_1 + q_2B_2 + r_2) + (p_3A_2 + q_3B_1 + r_3 + p_4A_2 + q_4B_2 + r_4)]\} = 0 \textbf{(A.8)}$$

$$[(p_1A_1 + q_1B_1 + r_1 + p_2A_1 + q_2B_2 + r_2) + (p_3A_2 + q_3B_1 + r_3 + p_4A_2 + q_4B_2 + r_4)] = T \quad \textbf{(A.9)}$$

Similarly, for the conditions $\frac{\partial E}{\partial p_2} = 0$, $\frac{\partial E}{\partial p_3} = 0$, $\frac{\partial E}{\partial p_4} = 0$, $\frac{\partial E}{\partial q_1} = 0$, $\frac{\partial E}{\partial q_2} = 0$, $\frac{\partial E}{\partial q_3} = 0$, $\frac{\partial E}{\partial p_4} = 0$, $\frac{\partial E}{\partial r_1} = 0$, $\frac{\partial E}{\partial r_2} = 0$, $\frac{\partial E}{\partial r_3} = 0$, $\frac{\partial E}{\partial r_4} = 0$, we obtain the relations similar to (A.9).

These 12 equations are to be solved to obtain the consequent parameters. The simultaneous equations are written in matrix form.

$$\begin{pmatrix} A_1 & A_1 & A_2 & A_2 & B_1 & B_2 & B_1 & B_2 & 1 & 1 & 1 & 1 \\ A_1 & A_1 & A_2 & A_2 & B_1 & B_2 & B_1 & B_2 & 1 & 1 & 1 & 1 \\ A_1 & A_1 & A_2 & A_2 & B_1 & B_2 & B_1 & B_2 & 1 & 1 & 1 & 1 \\ A_1 & A_1 & A_2 & A_2 & B_1 & B_2 & B_1 & B_2 & 1 & 1 & 1 & 1 \\ A_1 & A_1 & A_2 & A_2 & B_1 & B_2 & B_1 & B_2 & 1 & 1 & 1 & 1 \\ A_1 & A_1 & A_2 & A_2 & B_1 & B_2 & B_1 & B_2 & 1 & 1 & 1 & 1 \\ A_1 & A_1 & A_2 & A_2 & B_1 & B_2 & B_1 & B_2 & 1 & 1 & 1 & 1 \\ A_1 & A_1 & A_2 & A_2 & B_1 & B_2 & B_1 & B_2 & 1 & 1 & 1 & 1 \\ A_1 & A_1 & A_2 & A_2 & B_1 & B_2 & B_1 & B_2 & 1 & 1 & 1 & 1 \\ A_1 & A_1 & A_2 & A_2 & B_1 & B_2 & B_1 & B_2 & 1 & 1 & 1 & 1 \\ A_1 & A_1 & A_2 & A_2 & B_1 & B_2 & B_1 & B_2 & 1 & 1 & 1 & 1 \\ A_1 & A_1 & A_2 & A_2 & B_1 & B_2 & B_1 & B_2 & 1 & 1 & 1 & 1 \end{pmatrix} \begin{pmatrix} p_1 \\ p_2 \\ p_3 \\ p_4 \\ q_1 \\ q_2 \\ q_3 \\ q_4 \\ r_1 \\ r_2 \\ r_3 \\ r_4 \end{pmatrix} = \begin{pmatrix} T \\ T \\ T \\ T \\ T \\ T \\ T \\ T \\ T \\ T \\ T \\ T \end{pmatrix} \textbf{(A.10)}$$

$$\begin{pmatrix} p_1 \\ p_2 \\ p_3 \\ p_4 \\ q_1 \\ q_2 \\ q_3 \\ q_4 \\ r_1 \\ r_2 \\ r_3 \\ r_4 \end{pmatrix} = \begin{pmatrix} A_1 & A_1 & A_2 & A_2 & B_1 & B_2 & B_1 & B_2 & 1 & 1 & 1 & 1 \\ A_1 & A_1 & A_2 & A_2 & B_1 & B_2 & B_1 & B_2 & 1 & 1 & 1 & 1 \\ A_1 & A_1 & A_2 & A_2 & B_1 & B_2 & B_1 & B_2 & 1 & 1 & 1 & 1 \\ A_1 & A_1 & A_2 & A_2 & B_1 & B_2 & B_1 & B_2 & 1 & 1 & 1 & 1 \\ A_1 & A_1 & A_2 & A_2 & B_1 & B_2 & B_1 & B_2 & 1 & 1 & 1 & 1 \\ A_1 & A_1 & A_2 & A_2 & B_1 & B_2 & B_1 & B_2 & 1 & 1 & 1 & 1 \\ A_1 & A_1 & A_2 & A_2 & B_1 & B_2 & B_1 & B_2 & 1 & 1 & 1 & 1 \\ A_1 & A_1 & A_2 & A_2 & B_1 & B_2 & B_1 & B_2 & 1 & 1 & 1 & 1 \\ A_1 & A_1 & A_2 & A_2 & B_1 & B_2 & B_1 & B_2 & 1 & 1 & 1 & 1 \\ A_1 & A_1 & A_2 & A_2 & B_1 & B_2 & B_1 & B_2 & 1 & 1 & 1 & 1 \\ A_1 & A_1 & A_2 & A_2 & B_1 & B_2 & B_1 & B_2 & 1 & 1 & 1 & 1 \\ A_1 & A_1 & A_2 & A_2 & B_1 & B_2 & B_1 & B_2 & 1 & 1 & 1 & 1 \end{pmatrix}^{-1} \begin{pmatrix} T \\ T \\ T \\ T \\ T \\ T \\ T \\ T \\ T \\ T \\ T \\ T \end{pmatrix} \textbf{(A.11)}$$